Macromolecular Research, Vol. 21, No. 1, pp 65-70 (2013)
DOI 10.1007/s13233-013-1009-6

www.springer.com/13233
pISSN 1598-5032 eISSN 2092-7673

Enhanced Performance of Organic Photovoltaic Devices by Photo-Crosslinkable Buffer Layer

Nam Su Kang[1,3], Mai Ha Hoang[2], Dong Hoon Choi[2], Byeong-Kwon Ju*[,1], Jae-Min Hong[3], and Jae-Woong Yu*[,4]

[1]*Display and Nanosystem Laboratory, College of Engineering, Korea University, Seoul 136-713, Korea*
[2]*Department of Chemistry, Advanced Materials Chemistry Research Center, Korea University, Seoul 136-701, Korea*
[3]*Future Convergence Research Division, Korea Institute of Science and Technology, Seoul 130-650, Korea*
[4]*Department of Advanced Materials Engineering for Information & Electronics, Kyung Hee University, Gyeonggi 446-701, Korea*

Received February 1, 2012; Revised March 21, 2012; Accepted April 27, 2012

Abstract: The performance of organic photovoltaic devices was enhanced by insertion of the photo-crosslinkable buffer layer. This buffer layer was formed by a photo curable precursor with bithiophene and pentadienyl moieties. The fill factor of the device with this buffer layer exceeded 0.7 in the organic photovoltaic cell. The characteristic of the photo-crosslinkable property enabled this buffer layer to be inserted between the hole extraction layer and the active layer, which formed an ohmic contact with both layers. The insertion of the buffer layer induced a 20% enhancement in conversion efficiency by small increases in the short-circuit current and the open-circuit voltage, and a huge increase in the fill factor. This photo-crosslinkable buffer layer acted as a leakage current reducing layer as measured by the reduced dark current. The high crystallinity and smooth surface of this buffer layer resulted in improved surface morphology and internal packing, thus enhanced the fill factor.

Keywords: organic photovoltaic, fill factor, photo-crosslinkable buffer layer.

Introduction

Organic photovoltaics (OPVs) are regarded as a cost-effective device capable of providing cheaper and eco-friendly renewable energy, which constitutes a viable alternative to fossil energy resources. The advantage of OPV is that it can be fabricated in flexible form by various advanced technologies such as printing technology, and the utilization of roll-to-roll processing would reduce the production cost further.[1-3] Recent rapid improvements in power conversion efficiency have raised hopes for commercial OPV devices. However, the conversion efficiency should be improved to its maximum value of approximately 11%.[4-6]

Due to the relatively low conversion efficiency of OPV devices, however, OPVs need to be fabricated in a large-scale photoactive area in order to achieve the desired power output.[7-9] The performance of a single OPV cell decreases with the incensement of the active area, because of the high resistivity caused by the increase of the series resistance and the decrease of the fill factor. The close relationship between the device area and the conversion efficiency is now well established. In order to achieve the maximum power conversion efficiency for a large active area device, it is important to enhance the fill factor of a single cell. The fill factor is related to the actual maximum obtainable power and represents the degree of current produced by light that is not dissipated in internal loses. In order to have a high fill factor, the device should have a low series resistance and a high shunt resistance.

The typical method of improving the fill factor in device fabrication is slow evaporation of the metal electrode.[10] The fill factor is sensitive to the active material-metal interface morphology. Therefore, fast metal evaporation causes interface inhomogeneity, thus resulting in the reduction of the fill factor.[11] There have been many reported attempts to achieve a higher fill factor. The first method was slow evaporation of solvent (*i.e.* drying) to form a device with better polymer morphology,[12] and the reported fill factor for slow drying was 0.68. The second reported method was the utilization of a thermal treatment to obtain the optimum morphology of two immiscible blends.[13] The reported fill factor for the appropriately prepared diode (*i.e.* optimized active layer morphology) was also 0.68. The third method was the utilization of an interfacial electron block layer/hole transporting layer (nickel oxide was deposited by pulsed-laser deposition).[14,15] The fill factor used for this interlayer study was 0.69, which is quite extreme value. Even though the

*Corresponding Authors. E-mails: jwyu@khu.ac.kr or bkju@korea.ac.kr

highest reported fill factor value is 0.72, this is very unusual value for a bulk heterojunction of poly(3-hexylthiophene) (P3HT) and methanofullerene (PCBM).[16] Typical values of the fill factor for a device fabricated with a bulk heterojunction of P3HT and PCBM are in the range between 0.5~0.66.

As described above, the use of a buffer layer is the excellent means of improving the fill factor. Due to the preparation characteristics of the OPV, which is an overlayed structure formed by solution processing; however, the use of a buffer layer is quite limited, because of the similar solubility of the solvents used during the overlaying process. In this work, we used a photo-crosslinkable precursor to form a buffer layer, and studied the influence of this buffer layer on the fill factor. The utilization of this kind of photo-crosslinkable precursor allows a layer-by-layer processing with the solution coating technique.

Experimental

A typical example of the sample preparation is as follows: 4.3 wt% of P3HT (purchased from Rieke Metals, EE grade) and PCBM (purchased from Nano-C) blend with a 1:0.6 ratio by weight was dissolved in anhydrous chlorobenzene and spin coated onto prepared PEDOT:PSS (PH500 series) coated ITO glass with/without a buffer layer at 2,500 rpm for 40 s. The thickness of the resulting active layer was 220 nm and it was pre-annealed at 150 ºC for 10 min. The 0.8 nm-thick LiF, which serves as a buffer layer for electron extraction, was deposited on top of the active layer and a 150 nm-thick aluminum layer was evaporated by thermal vapor deposition at 10^{-6}-10^{-7} Torr. The prepared device was post-annealed at 120 ºC for 10 min. The entire procedure was performed in a glove box with a high-purity nitrogen environment. The active cell areas were 0.04 cm^2. The solution (0.3 wt%) of 1,1-(5,5-(1E,1E)-2,2-(2,5-bis((E)-2-(5-hexyl-2,2-bithiophen-5-yl)vinyl)-1,4-phenylene)bis(ethene-2,1-diyl)-bis(2,2-bithiophene-5',5-diyl))bis(methylene) 4-di(penta-1,4-dien-3-yl) dibutanedioate (HB2P)[17] in chlorobenzene was spin coated onto PEDOT:PSS layer, and crosslinked organic semiconducting film was made by exposure on the film under UV light (254 nm, intensity=40.64 mW/cm^2) for 3 min at room temperature.

The thickness of the coated film was measured with a surface profiler (TENCOR®, P-10 α-step). The surface morphology of the samples was studied using a tapping mode atomic force microscope (Digital Instruments Multimode) equipped with a nanoscope IIIa controller. The absorption spectra of the films were obtained using a photodiode array type UV-vis spectrometer (HP 8453). An Oriel Class A type solar simulator (IEC 904) with an Oriel Reference Cell (calibrated data traceable to NREL) was used as a light source. All of the measurements were performed under the 1 sun condition (AM 1.5 100 mW/cm^2). The measurements were not corrected for reflection losses or for light absorption in the ITO electrode. The *I-V* characteristics were determined with a Keithley 2400 source-measure unit, and a surface tensiometer (Krüss, K6) and drop shape analyzer (Krüss, DS-100) were used to analyze the surface and interfacial properties of the interfacial layers in the organic solar cell.

Results and Discussion

The chemical structure of the photo curable precursor (HB2P) used in this study is shown in Figure 1(a). This photo-crosslinkable precursor was designed to possess bithiophene moieties for a high carrier mobility characteristic and pentadienyl moieties for photo-crosslinking sites. The detailed synthesis of this precursor is described elsewhere.[15] According to the X-ray analysis, the hexyl peripheral groups interact between themselves by van der Waals

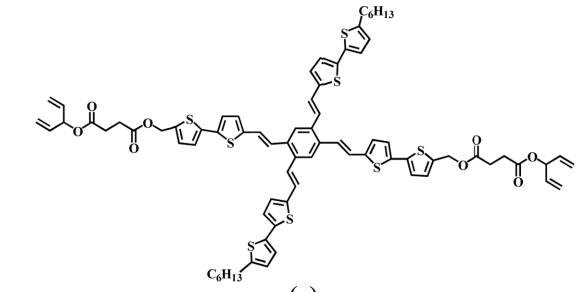

(a)

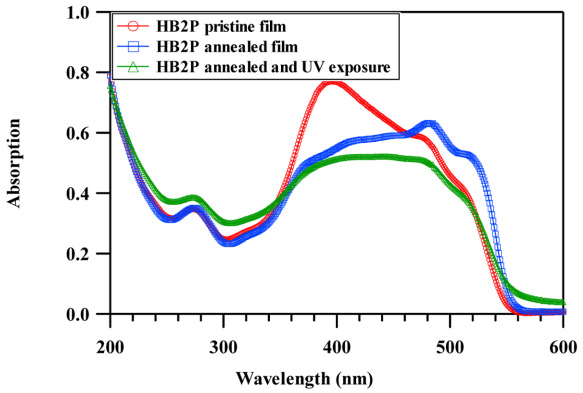

(b)

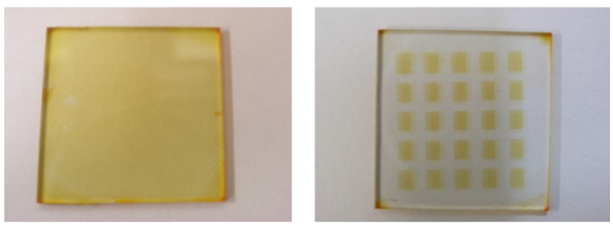

as prepared sample patterned sample

(c)

Figure 1. (a) The chemical structure of the UV crosslinkable precursor, (b) UV-vis spectral changes, and (c) the patterned film by UV crosslinkable system.

interaction, and enhance the intermolecular ordering to improve the crystallinity in HB2P. The studies of photo-crosslinking and the resulting solubility test are described elsewhere.[15] UV-Vis spectral changes due to the cure process are shown in Figure 1(b). In the UV-vis spectra of film state after annealing and UV exposure, the absorption spectrum of vibronic transitions is obscured which is typical spectral changes for crosslinked film, while pristine and annealed films show vibronic peaks. Insolubility of photo-crosslinked film was tested by formation of the patterned structure. The bare film before UV exposure prepared by spin coating on glass is shown in left picture, the patterned structure after UV exposure and cleaning of unexposed area by solvent is shown in right as shown in Figure 1(c). From this study, it is clear that the photo-crosslinking results an indissoluble film. The optimized devices for OPV studies were prepared on top of this crosslinked buffer layer as described in experimental section.

The energy levels (HOMO, LUMO and energy band gap) were studied using cyclicvoltamogram and UV-vis spectroscopy. The band energy diagrams are given in Figure 2. The HOMOs of the photo-crosslinked buffer layer material and the P3HT are very close to that of the PEDOT, which serves as the hole extraction layer, so these buffer layer can form an ohmic contact with the hole extraction layer and the active layer. As a result of this ohmic contact, the contact resistance and the barrier height could be minimized. Meanwhile, LUMOs of the buffer layer are bigger than that of P3HT or PCBM, therefore, this buffer layer can serve as an electron blocking layer. Band barrier should be considered in the view point of the separated charges. In other words, in the P3HT:PCBM blend system, the formed electron by charge separation will move through the PCBM cluster. The direct contact between PCBM and PEDOT can cause leakage problem. The energy level differences for electron transfer in devices with buffer layer should be accounted for the differences between LUMO of HB2P and PCBM, because electron will not go through P3HT due to very low electron mobility within P3HT. In other words, all the separated electrons will be located in PCBM cluster. Therefore the energy barrier for electron transfer is about 0.8 eV (LUMO

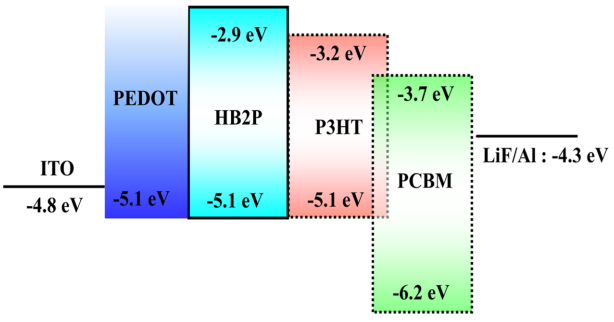

Figure 2. The band energy diagram.

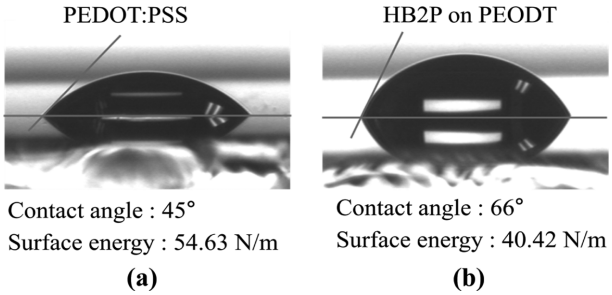

Figure 3. The contact angle studies; (a) PEDOT surface and (b) buffer layer surface.

level of PCBM is 3.7 eV and LUMO of HB2P is 2.9 eV) which is more than the energy require to break up the exciton. Therefore this energy barrier is big enough to act as an electron blocking layer. Insertion of this electron block layer can improve device performance by reducing charge quenching. As our experimental results indicated, it acted as an excellent leakage blocking layer so that the fill factor was exceeded 0.7 which is extremely high value.

In order to study the influence of the surface energy of these materials, we performed a contact angle study of the PEDOT surface and the photo-crosslinked buffer layer. As shown in Figure 3, the surface of the buffer layer is more hydrophobic, since the contact angle measurement of the PEDOT surface is 45º (calculated surface energy is 54.6 mN/m) while that of the buffer layer is 66º (calculated surface energy is 40.4 mN/m). Compared with the reported surface energy values of PCBM (37.8 mN/m) and P3HT (26.9 mN/m),[18] it is clear that this buffer layer will form a better interface with the active layer (blend of P3HT and PCBM) than that with PEDOT. Better adhesion is very important factor for enhanced device performance.

The surface roughness is another important factor affecting the fill factor of the device. Since the overall thickness of OPV devices is very thin (300~500 nm including metal electrode), any rough surface can affect the following overlayed layers. We used AFM to study the surface roughness of each layer and their effect on the overlayed layers. As shown in Figure 4, the RMS surface roughness of ITO glass (a) was about 3.5 nm. When PEDOT was over-coated on top of ITO, the RMS changed to 2.0 nm (b) and the buffer layer reduced the surface roughness further to 1.2 nm (c). The active layer coating on this buffer layer resulted in a much smoother surface (the surface RMS became 2.0 nm) than the one without the buffer layer (the surface RMS became 3.0 nm) as shown in Figure 4(d) and (e). The image analysis implies that the buffer layer caused the better surface roughness of the active layer, resulting in a nicer interface between these layers. The results of the contact angle study and the AFM surface study imply that this buffer layer will result in a better interface between the PEDOT and the active layer. The smoother surface will affect the

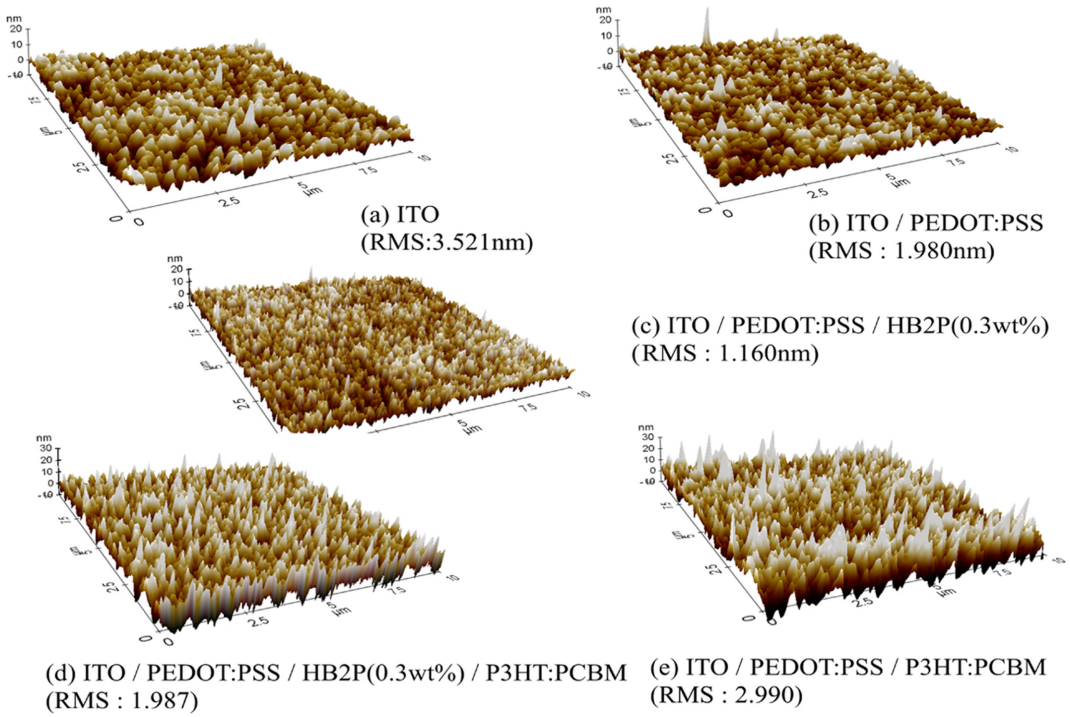

Figure 4. The AFM topography images; (a) Bare ITO surface, (b) ITO/PEDOT surface, (c) ITO/PEDOT/buffer layer, (d) ITO/PEDOT/buffer layer/active layer, and (e) ITO/PEDOT/active layer.

overall device performance.[19-21]

Figure 5(a) shows the *I-V* characteristics of the devices with and without buffer layer. The overall data are summarized in Table I. The open-circuit voltage, the short-circuit current density, the fill factor, and the power conversion efficiency under the AM 1.5 condition without buffer layer (*i.e.* the reference cell) were, 0.573 V, 9.11 mA/cm^2, 0.638, and 3.33%, respectively. When the ~5 nm thick photo-crosslinked buffer layer was inserted between the PEDOT and the active layer, these values changed to 0.600 V, 9.65 mA/cm^2, 0.704, and 4.05%, respectively. The power conversion efficiency of the buffer layer device increased by about 20% compared to that of the cell without buffer layer. The major reason for this enhancement was the increase in the fill factor. Figure 5(b) shows the logarithmic *I-V* characteristic plots of the device with and without buffer layer. As shown in figure, the with-buffer-layer device showed a lower dark current while it had a higher photocurrent than the one without buffer layer. The plot clearly shows that the buffer layer prevented shunt leakage in the dark state.

Even though the open-circuit voltage represents the built-in potential in fabricated devices, which is mainly determined by the energy difference between the HOMO of the donor material and the LUMO of the acceptor material, this should also depend on the fabrication techniques. The theoretical maximum open-circuit voltage of a bulk heterojunction of poly(3-hexylthiophene) (P3HT) and methanofullerene is 0.62±0.03 V.[22] Since this buffer layer offers a better diode

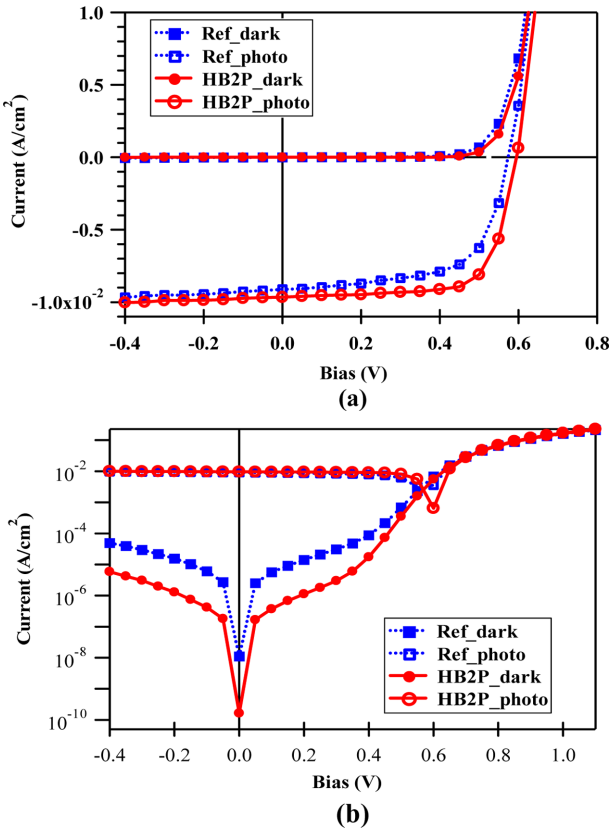

Figure 5. (a) The *I-V* characteristics of the device and (b) The log *I-V* plots of the device.

Table I. Device Performance Table of Reference Cell and Organic Solar Cell with Photo-Crosslinkable Buffer Layer (HB2P)

	V_{oc} (V)	J_{sc} (mA/cm^2)	Fill Factor	EFF (%)	Series Resist (Ωcm^2)	Shunt Resist (Ωcm^2)
Ref	0.573 (±0.01)	9.11 (±0.2)	0.638 (±0.02)	3.33 (±0.2)	3.05	7.33×10^3
HB2P	0.600 (±0.01)	9.65 (±0.3)	0.704 (±0.01)	4.05 (±0.1)	2.72	4.72×10^4

factor environment due to its smoothness and close-packed crystalline film, causing an enhanced adhesion, enhanced open-circuit voltage is expected for the with-buffer-layer device. Due to the characteristics of this buffer layer for the prevention of leakage current, there will be an additional increase in the open-circuit voltage due to the increase in shunt resistance. As expressed in Table I, the open-circuit voltage was increased from 0.573 V for the reference device to 0.60 V for the buffer-layer device.[18,23]

The shunt resistance and series resistance of the device measured from the *I-V* plot (Figure 5(a)) was 7.33×10^3 and 3.05 Ωcm^2 for the without-buffer-layer device (reference device) and 4.72×10^4 and 2.72 Ωcm^2 for the with-buffer-layer device. The data are also summarized in Table I. From these resistance values (increase in the shunt resistance and decrease in the series resistance), it is also clear that this buffer layer plays the role of a leakage current preventing layer. The most noticeable change in the devices was the fill factor. The shunt resistance representing the device rectification was improved noticeably, as shown in Figure 5(a), resulting in the fill factor increasing from 0.638 for the reference cell to 0.704 for the with-buffer-layer device.

Figure 6 shows the incident photon to current collection efficiency (IPCE) spectrum of devices with and without buffer layer. The reference device shows the typical spectral response of the P3HT:PCBM blend film with a maximum IPCE of ~66% at 516 nm, which is similar to other reports.[24] For the with-buffer-layer device, the extracted current was almost identical to that of the reference device, except that the buffer layer absorption (as shown in Figure 1(b), HB2P absorption maximum is near 400 nm) contributed minor currents. When

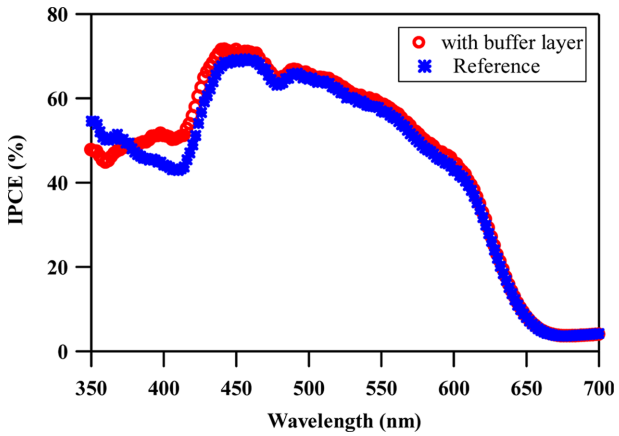

Figure 6. The IPCE plots of the device with and without buffer layer.

we compare two IPCE spectra for with and without the buffer layer, IPCE at 400 nm is less than 5% in that wavelength. The total contribution has to be counted for the area underneath all IPCE spectrum, and the contribution from HB2P, in other words charge formed by HB2P absorption, is much less than 1% of the total IPCE spectrum area. These IPCE measurements imply that devices that fabricated with and without buffer layer are identically prepared (which means identical light absorption and charge generation) except that there is a buffer layer, which can enhance the device rectification. Therefore it can be concluded that this buffer layer enhances the device rectification from the facts that increase in shunt resistance about 8 time with the buffer layer compare to without the buffer layer as calculated in Table I (Shunt resistance for with buffer layer is 4.72×10^4 Ωcm^2 and that for without buffer layer is 7.33×10^4 Ωcm^2). Shunt resistance and the fill factor are the main criteria for the measure of rectification by the increase in shunt resistance (4.72×10^4 to 7.33×10^4 Ωcm^2) and the enhanced fill factor (0.638 to 0.704) as summarized in Table I.

Conclusions

The performance of organic photovoltaic devices was enhanced by insertion of the photo-crosslinkable buffer layer. In order to enhance the performance of OPVs, it is very important to have a well-fabricated device that will reach maximum expected capability, even in a large-area device. In this study, we used a photo-crosslinkable buffer layer, which is prepared *via* layer-by-layer processing with the solution coating technique. This buffer layer acts as a leakage current reducing layer and it played an important role in enhancing rectification. This buffer layer showed a high crystallinity and smoother surface, resulting in a better surface morphology, and enhanced internal packing resulting in an enhanced fill factor. From this study, we could conclude that this buffer layer enhance the device rectification by the increase in shunt resistance (4.72×10^4 to 7.33×10^4 Ωcm^2) and the enhanced fill factor (0.638 to 0.704) as summarized in Table I. "The best application process of this method is the leakage current control buffer for conventional type OPVs so that it can enhance the fill factor as shown in this study; however, this method cannot be used in invert type OPV since the buffer layer coating process can dissolve the active layer which coated before the hole extraction layer (PEDOT layer) due to the similarity in solubility."

Acknowledgment. This work was supported by a grant from Kyung Hee University in 2010 (KHU-20100607).

References

(1) D. Wohrle and D. Meissner, *Adv. Mater.*, **3**, 129 (1991).
(2) N. S. Sariciftci, C. J. Brabec, and J. C. Hummelen, *Adv. Funct. Mater.*, **11**, 15 (2001).
(3) T. Ameri, G. Dennler, C. Lungenschmied, and C. J. Brabec, *Energy Environ. Sci.*, **2**, 347 (2009).
(4) M. C. Scharber, D. Wuhlbacher, M. Koppe, P. Denk, C. Waldauf, A. J. Heeger, and C. L. Brabec, *Adv. Mater.*, **18**, 789 (2006).
(5) C. J. Brabec, G. Dennler, and M. C. Scharber, *Adv. Mater.*, **21**, 1323 (2009).
(6) K. Lee, S. H. Park, A. Roy, S. Beaupre, S. Cho, N. Coates, J. S. Moon, D. Moses, M. Leclerc, and A. J. Heeger, *Nat. Photonics*, **3**, 297 (2009).
(7) L. Blankenburg, K. Schultheis, H. Schache, S. Sensfuss, and M. Schrodner, *Sol. Energy Mat. Sol. Cells*, **93**, 476 (2009).
(8) F. C. Krebs, M. Manceau, D. Angmo, and M. Jorgensen, *Org. Electron.*, **12**, 566 (2011).
(9) J. H. Kwon, H.-D. Yeo, H.-J. Cha, M. J. Lee, H.-T. Park, J.-H. Park, C.-E. Park, and Y.-H. Kim, *Macromol. Res.*, **19**, 197 (2011).
(10) D. Gupta, M. Bag, and K. S. Narayan, *Appl. Phys. Lett.*, **92**, 093301 (2008).
(11) M. Glatthaar, M. Riede, N. Keegan, K. Sylvester-Hvid, B. Zimmermann, M. Niggemann, A. Hinsch, and A. Gombert, *Sol. Energy Mat. Sol. Cells*, **91**, 390 (2007).
(12) Y. Yang, G. Li, V. Shrotriya, J. S. Huang, Y. Yao, T. Moriarty, and K. Emery, *Nat. Mater.*, **4**, 864 (2005).
(13) A. J. Heeger, W. L. Ma, C. Y. Yang, X. Gong, and K. Lee, *Adv. Funct. Mater.*, **15**, 1617 (2005).
(14) R. P. H. Chang, M. D. Irwin, B. Buchholz, A. W. Hains, and T. J. Marks, *Proc. Natl. Acad. Sci. U.S.A.*, **105**, 2783 (2008).
(15) M. Shin, H. Kim, and Y. Kim, *Macromol. Res.*, **18**, 709 (2010).
(16) G. H. Kim, H. K. Song, and J. Y. Kim, *Sol. Energy Mat. Sol. Cells*, **95**, 1119 (2011).
(17) M. H. Hoang, M. J. Cho, D. C. Kim, K. H. Kim, J. W. Shin, M. Y. Cho, J. S. Joo, and D. H. Choi, *Org. Electron.*, **10**, 607 (2009).
(18) D. Gupta, M. Bag, and K. S. Narayan, *Appl. Phys. Lett.*, **92** (2008).
(19) S. E. Shaheen, C. J. Brabec, N. S. Sariciftci, F. Padinger, T. Fromherz, and J. C. Hummelen, *Appl. Phys. Lett.*, **78**, 841 (2001).
(20) N. S. Kang, B. K. Ju, T. W. Lee, J. M. Hong, D. H. Choi, and J.-W. Yu, *Sol. Energy Mat. Sol. Cells*, **95**, 2831 (2011).
(21) K.-J. Kim, Y.-S. Kim, W.-S. Kang, B.-H. Kang, S.-H. Yeom, D.-E. Kim, J.-H. Kim, and S.-W. Kang, *Sol. Energy Mat. Sol. Cells*, **94**, 1303 (2010).
(22) K. Vandewal, K. Tvingstedt, A. Gadisa, O. Inganas, and J. V. Manca, *Nat. Mater.*, **8**, 904 (2009).
(23) X. R. Tong, B. E. Lassiter, and S. R. Forrest, *Org. Electron.*, **11**, 705 (2010).
(24) K. Lee, J. Y. Kim, S. H. Kim, H. H. Lee, W. L. Ma, X. Gong, and A. J. Heeger, *Adv. Mater.*, **18**, 572 (2006).